Research Article

Junzhong Wang, Jiaqi Zhu, Yiqi Jiang, Mengying Li, Kuai Yu* and Guo Ping Wang*

Observation of elastic heterogeneity and phase evolution in 2D layered perovskites using coherent acoustic phonons

https://doi.org/10.1515/nanoph-2021-0358
Received July 9, 2021; accepted October 12, 2021;
published online October 27, 2021

Abstract: Two-dimensional (2D) organic–inorganic perovskites have shown interesting optical properties due to the natural quantum-well structures. The repetition of soft organic and hard inorganic intercalations also renders 2D perovskites rich phonon dynamics. Here, we investigated the coherent acoustic phonons in $(PEA)_2PbI_4$ perovskite films by time-resolved Brillouin spectroscopy. The coherent acoustic phonons were launched indirectly in perovskite films by exciting Au nanoplates which were used as optoacoustic transducers. A longitudinal sound velocity $v = 1937 \pm 31$ m/s, and an elastic modulus $E = 9.84$ GPa along the cross-plane direction of perovskites were obtained from analysis of the Brillouin oscillation frequency. Following a bead-spring model, we calculated a spring constant $k \approx 1.709$ N m^{-1} for PEA cations which is comparably small for perovskites. We also demonstrated that coherent acoustic phonons are sensitive to differentiate structural heterogeneity and monitor dynamic phase evolution in perovskite films. Domains of PbI_2-rich and PbI_2-poor phases were identified. Under light stimulus, PbI_2-poor phases were gradually disappearing and PbI_2-rich phases became crystallized. The observations of structural and elastic heterogeneity and dynamic phase evolution using coherent acoustic phonons provide a toolbox for submicroscale elastic characterization of perovskites.

Keywords: acoustic phonon; elastic heterogeneity; perovskite; time-domain Brillouin spectroscopy.

Junzhong Wang and Jiaqi Zhu contributed equally to this work.

***Corresponding authors: Kuai Yu and Guo Ping Wang**, Institute of Microscale Optoelectronics, Shenzhen University, Shenzhen 518060, China, E-mail: kyu@szu.edu.cn (K. Yu), gpwang@szu.edu.cn (G. P. Wang). https://orcid.org/0000-0001-6138-0367 (K. Yu)
Junzhong Wang, Jiaqi Zhu, Yiqi Jiang and Mengying Li, Institute of Microscale Optoelectronics, Shenzhen University, Shenzhen 518060, China

1 Introduction

Hybrid organic–inorganic halide perovskites have attracted enormous attention in photovoltaics and optoelectronic applications, including solar cells, light-emitting diodes, and photodetectors [1–3], due to their large light absorption coefficients, high photoluminescence quantum yields, tunable wide spectral ranges, and low-cost solution manufacturing processes [4–6]. Unfortunately, the poor stability and degradation due to reactivity with oxygen and water as well as internal ion migration under ambient conditions hinder their potential applications [7]. Two-dimensional (2D) Ruddlesden–Popper (RP) organic–inorganic perovskites have shown greater resistance to degradation due to the hydrophobic organic layers, which block water and oxygen invasions into the perovskite crystals [8, 9]. One of the most widely employed organic layers for 2D RP perovskites is phenethylammonium ($C_6H_5C_2H_4NH_3$, or PEA) which separates the inorganic layers and facilitates the formation of multiquantum well structures [10]. The repetition of soft organic and hard inorganic intercalations renders the 2D perovskites exceptionally interesting electron and phonon dynamics, such as prolonged hot-carrier lifetimes and the formation of large polarons [11–15].

Despite 2D RP perovskites as alternatives to 3D counterparts have exhibited superior optical and phonon properties, they still suffer from structural inhomogeneity and instability [16, 17]. Fundamental understanding of structural changes and evolution under relevant in operando conditions is essential to effectively improve the lifetimes of perovskite devices and tailor their photophysical properties. Multimodal microscopy approaches have been utilized to better understand and exploit perovskite heterogeneities [17]. Combination of photoluminescence and lifetime imaging, cathodoluminescence, infrared photothermal heterodyne imaging, Brillouin spectroscopy, compositional X-ray microscopy, as well as scanning and transmission electron microscopy were shown excellent capabilities to decipher structural heterogeneities [18–23]. Time-domain Brillouin microscopy or picosecond ultrasonics has been

demonstrated in high-resolution structural characterizations for many fields from material science to biology [24, 25]. However, applications of coherent acoustic phonons for the characterization of perovskites are less explored, compared to the studies of optical phonons [26–28].

Time-domain Brillouin spectroscopy based on femtosecond pump–probe experimental technique provides an all-optical method for structural characterizations [24]. In pump–probe experiments, a pump pulse laser is absorbed by an optoacoustic transducer, resulting in generation of coherent acoustic phonons traveling in the material. A time delayed probe laser is used to monitor the propagation of acoustic strains by detecting reflected light where an oscillating signal is presented due to interference between light reflected from stationary surfaces and propagating acoustic strains [29–31]. The time-domain oscillation pattern is commonly called Brillouin oscillations and the frequency f_b depends on refractive index (n) and longitudinal speed of sound (v) of the material: $f_b = 2vn\cos\phi/\lambda_{pr}$, where λ_{pr} is the probe wavelength and φ is the angle of incidence of the probe beam. Under normal incidence, the frequency expression reduces to $f_b = 2vn/\lambda_{pr}$ [29, 32]. In order to be able to differentiate structural inhomogeneity in perovskites, it is desirable to have a significant frequency shift $\Delta f/f_b = \Delta n/n$ in terms of refractive index. Earlier studies have shown that structural inhomogeneity (Δn) leads to evident absorption and photoluminescence (PL) shifts at the energy bandgap [16, 33, 34]. Probing the Brillouin oscillations at energy bandgap thus gives the optimal sensitivity to monitor structural heterogeneity and evolution.

In this work, we have demonstrated that coherent acoustic phonons can probe the structural inhomogeneity and ion migrations in phenethylammonium lead iodide ($(PEA)_2PbI_4$) perovskites which were used as a model to investigate structural response under environmental stresses. The coherent acoustic phonons were launched in perovskites by exciting single Au nanoplates (NPLs) which were deposited on surface of the film and used as optoacoustic transducers. Propagation of coherent acoustic phonons in perovskites was detected in time-resolved Brillouin microscopy with probe wavelength of 530 nm that is close to the energy bandgap. A single Brillouin oscillation frequency $f_b = 18.9 \pm 0.5$ GHz was obtained for homogeneous $(PEA)_2PbI_4$ perovskites. A longitudinal sound velocity $v = 1937 \pm 31$ m/s and an elastic modulus $E = 9.84$ GPa along cross-plane direction were calculated. Mode splitting of the Brillouin peak was observed that was strongly related to perovskite film heterogeneity. Domains of PbI_2-rich and PbI_2-poor phases were identified. Moreover, light-induced ion migrations and formation of PbI_2 phase were observed. The measurements show that coherent acoustic phonons present an all-optical characterization of dynamic disorders in perovskites.

2 Results and discussion

$(PEA)_2PbI_4$ perovskite films and Au NPLs were both chemically synthesized based on previously described methods [14, 35]. The detailed synthesis procedures are given in Experimental methods section. The $(PEA)_2PbI_4$ perovskites were spin-coated and crystalized on glass substrates. The schematic crystal structure is shown in Figure 1a, where the 2D RP organic–inorganic hybrid structure consists of sheets of corner-sharing Pb-I octahedra expanding in two dimensions, separated by interdigitating bilayers of organic PEA cations. The structure was demonstrated highly efficient to block heat-carrying, low-energy acoustic phonons propagation along the cross-plane direction. The liquid-like motion of organic cations and large acoustic impedance mismatch at organic–inorganic interfaces are the dominant factors in impeding acoustic phonon transport [11, 36]. Study of coherent acoustic phonons in 2D perovskites will guide the design of more energy efficient devices.

Au NPLs with thicknesses of 10–20 nm and edge lengths of 10–20 μm were synthesized and deposited on surface of perovskite films (schematically shown in Figure 1a). Figure 1b shows a representative scanning electron microscopy (SEM) image of a single Au NPL on $(PEA)_2PbI_4$ perovskites, where the film surface is relatively smooth and Au NPL is in intimate contact with the perovskites. The crystal structure and orientation of $(PEA)_2PbI_4$ perovskite film on glass substrate was characterized by X-ray diffraction (XRD), as shown in Figure 1c. The spectrum indicates that the film has well-defined diffraction peaks corresponding to (00l) (l = 2, 4, 6, 8, 10 and 12) series of reflections, which is consistent with previous reports that $(PEA)_2PbI_4$ film has 2D layered structures with Pb-I octahedra sheets parallel to the substrate [37, 38]. The strong and sharp diffraction orders indicate excellent crystallinity of perovskites. A lattice distance $d = 1.61$ Å between layers of inorganic Pb-I octahedra sheets was calculated, which is consistent with reported values. Figure 1d displays the UV-visible absorption and PL spectroscopy of $(PEA)_2PbI_4$ perovskites that exhibit a strong absorption band at ~516 nm and a narrow emission at ~532 nm [39]. The spectra also indicate the successful formation of $(PEA)_2PbI_4$ perovskites [40, 41].

Coherent acoustic phonons in perovskites were launched indirectly by exciting single Au NPLs with femtosecond laser pulses and detected by a time-delayed

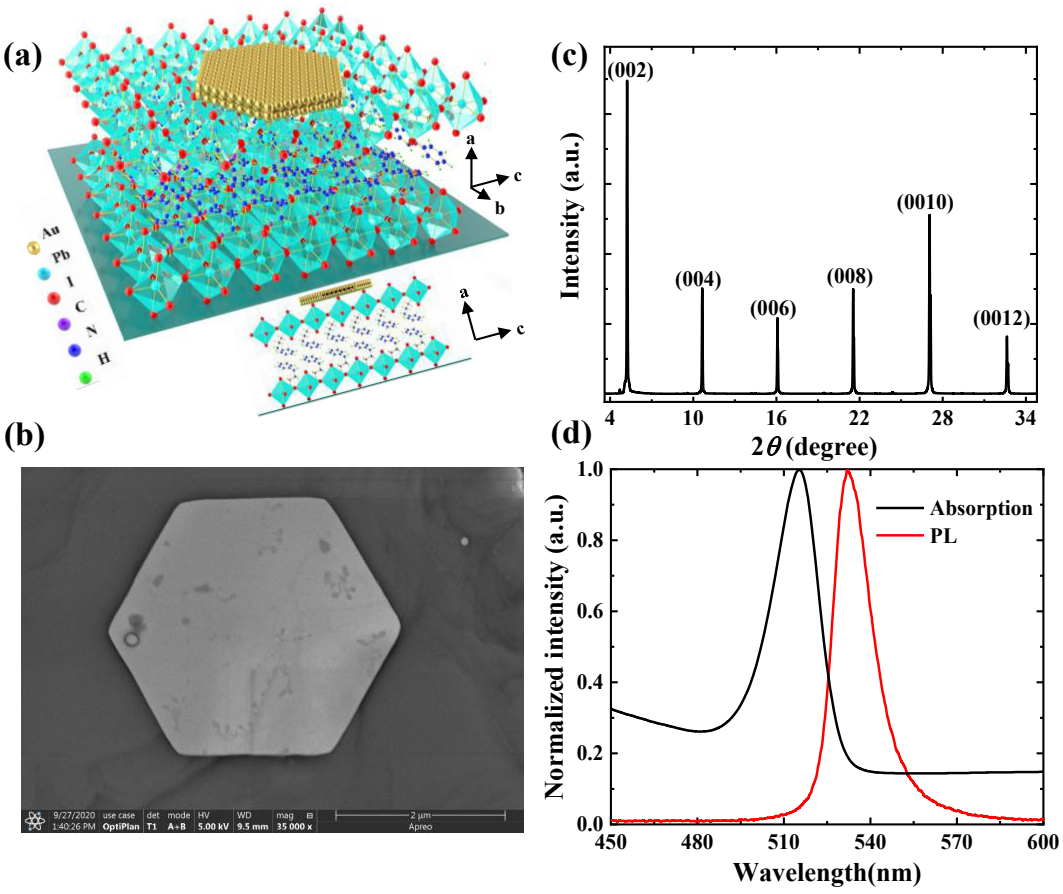

Figure 1: Spectroscopic characterization of $(PEA)_2PbI_4$ perovskite films.
(a) Schematic diagram of sample configuration where Au NPLs were deposited on surface of perovskites for the generation of coherent acoustic phonons. The perovskite film was spin-coated on glass substrate. (b) SEM image of an area of perovskite film with a Au NPL on top. (c) XRD spectrum, and (d) UV–Vis absorption (black line) and photoluminescence (red line) spectra of the perovskite film.

probe laser in a pump-probe scheme (see Experimental methods for details) [24, 29]. Previously, thin Au nanoplates were demonstrated to be potential and easily deployable optoacoustic transducers [29]. The advantages of using chemically synthesized Au NPLs to generate acoustic phonons are the broad applicability of plasmonic nanoparticles. In the current studies, the samples were excited and detected from the side of Au NPLs rather than the perovskites. This configuration minimizes the photodamage of perovskites. Propagation of coherent acoustic phonons in perovskite film was detected with pump-probe spectroscopy. Typical powers were 2.5 mW for the 800 nm pump beam and 50 μW for the 530 nm probe beam. Under these conditions, the detected Brillouin oscillations were stable.

Figure 2a shows a transient reflectivity trace of a single Au NPL on $(PEA)_2PbI_4$ film where a pronounced modulation of signal is observed over several hundred picoseconds. The red curve is a fitting to the damped Brillouin oscillations which gives a vibrational lifetime of ~300 ps. This relatively short lifetime could be due to limited penetration depth of the probe light at energy bandgap. The fast Fourier transform (FFT) spectrum of the modulation signal gives an oscillation frequency $f_b = 18.9 \pm 0.3$ GHz. The observed oscillations are assigned to Brillouin oscillations instead of acoustic vibration of Au NPL [29, 42]. This was confirmed by measuring the Brillouin oscillations with varied probe wavelengths from 530 to 600 nm. The measured vibrational frequencies are shown in Figure 2b and the corresponding transient reflectivity signals are presented in Supporting Information Figure S1. The FFT spectra are shown in Supporting Information Figure S2. Note that the localized acoustic vibration of the Au NPL was not observed where the frequency is NPL thickness dependent and irrelevant to the probe wavelength [29, 42]. The completely damping of localized acoustic vibration of Au NPL and the formation of propagating acoustic phonons demonstrate that Au NPL is mechanically coupled to perovskites.

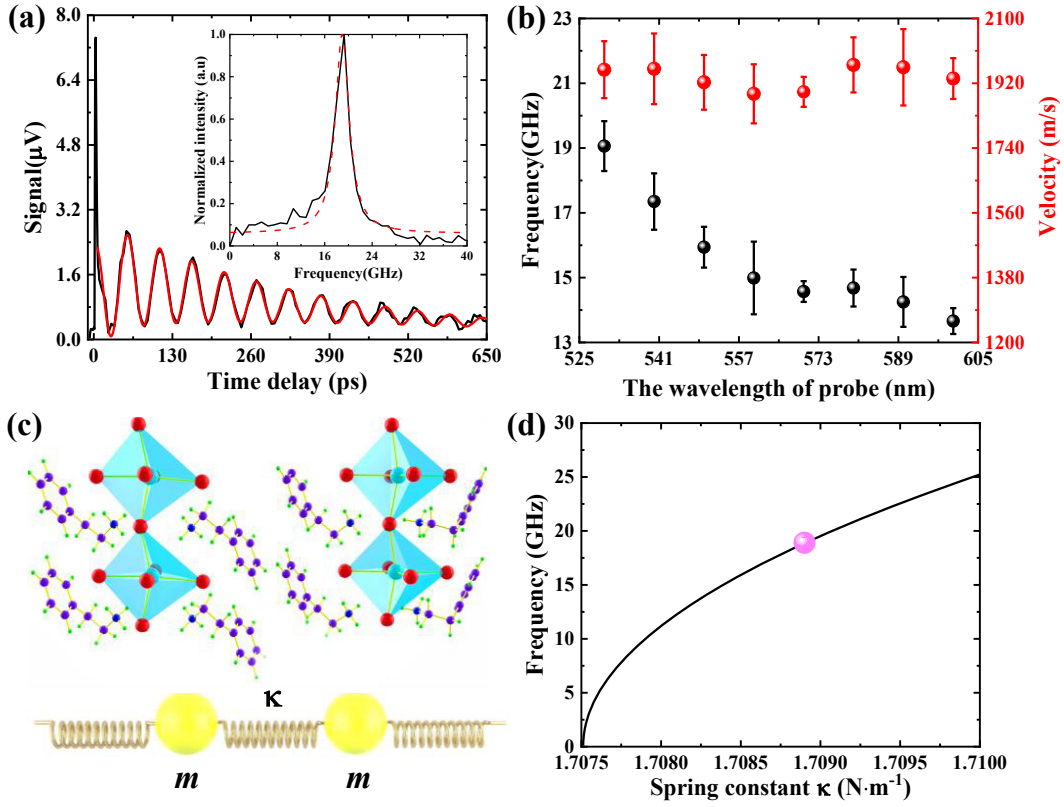

Figure 2: Coherent acoustic phonons in perovskites.
(a) Transient reflectivity trace for a single Au NPL on $(PEA)_2PbI_4$ film where Brillouin oscillations were observed with pump and probe wavelengths of 800 and 530 nm, respectively. The red is a fit to the curve which gives phonon lifetime of 300 ps. Inset shows the fast Fourier transform (FFT) spectrum of the oscillations together with a Lorentz curve fitting in red. (b) Probe wavelength dependent Brillouin oscillation frequency and the calculated sound wave velocities with average value of $v = 1937 \pm 31$ m/s (error stands for standard deviation). (c) Schematic illustration of the bead-spring model in $(PEA)_2PbI_4$ film. (d) Calculated spring constant k versus acoustic phonon frequency. The marker is the experimental measurement in $(PEA)_2PbI_4$ perovskites.

The frequency of Brillouin oscillations is given by $f_b = 2vn/\lambda_{pr}$, which depends on refractive index and sound velocity of the medium [24, 29, 36, 43, 44]. The wavelength dependent refractive index n of $(PEA)_2PbI_4$ was adopted from previous data and was shown in Supporting Information Figure S3 [45, 46]. Using the refractive index and measured Brillouin oscillation frequency, we calculated a longitudinal speed of sound $v = 1937 \pm 31$ m/s and the results are plotted in Figure 2b. The cross-plane sound velocity is slightly smaller than literature value 2100 m/s for $(PEA)_2PbI_4$ single crystals, but much larger than the value 1476 m/s for $(BA)_2PbI_4$ single crystals [36, 43]. Furthermore, an elastic constant was calculated $E = 9.84$ GPa, using equation $E = \rho v^2$ with $\rho = 2.622$ g/cm^3 being the density of $(PEA)_2PbI_4$ perovskites [13]. Compared to 3D perovskites, the relatively small sound velocity and elastic constant indicate the softness of crystal lattices of 2D RP perovskites, which are in good agreement with previous reports [22, 36, 43, 44]. To gain insights of coherent acoustic phonon propagation along cross-plane direction of 2D perovskites, we illustrate the interaction among layers using one dimensional bead-spring model following the work done by Guo et al.[36]. The model is schematically presented in Figure 2c. Each bead represents a single Pb-I octahedron in the model, which was linked by PEA cations with spring constant k. In the model, the distance d = 16.1 Å is determined from the XRD spectrum and the weight of single Pb-I octahedron is $m_{PbI_4} = 1.187 \times 10^{-24}$ kg. The calculated spring constant k versus the acoustic phonon frequency is presented in Figure 2d. A value of $k \approx 1.709$ N m^{-1} matches the experimental results which is slightly larger than the spring constant 1.13 N m^{-1} of BA cations in $(CH_3(CH_2)_3NH_3)_2PbI_4$ perovskites [36]. A larger value of k also indicates the larger rigidity of PEA cations compared to BA and a higher acoustic phonon velocity in $(PEA)_2PbI_4$ perovskites.

Next we explore the possibility of using coherent acoustic phonons to investigate structural inhomogeneity in perovskites. Fluorescence was previously demonstrated

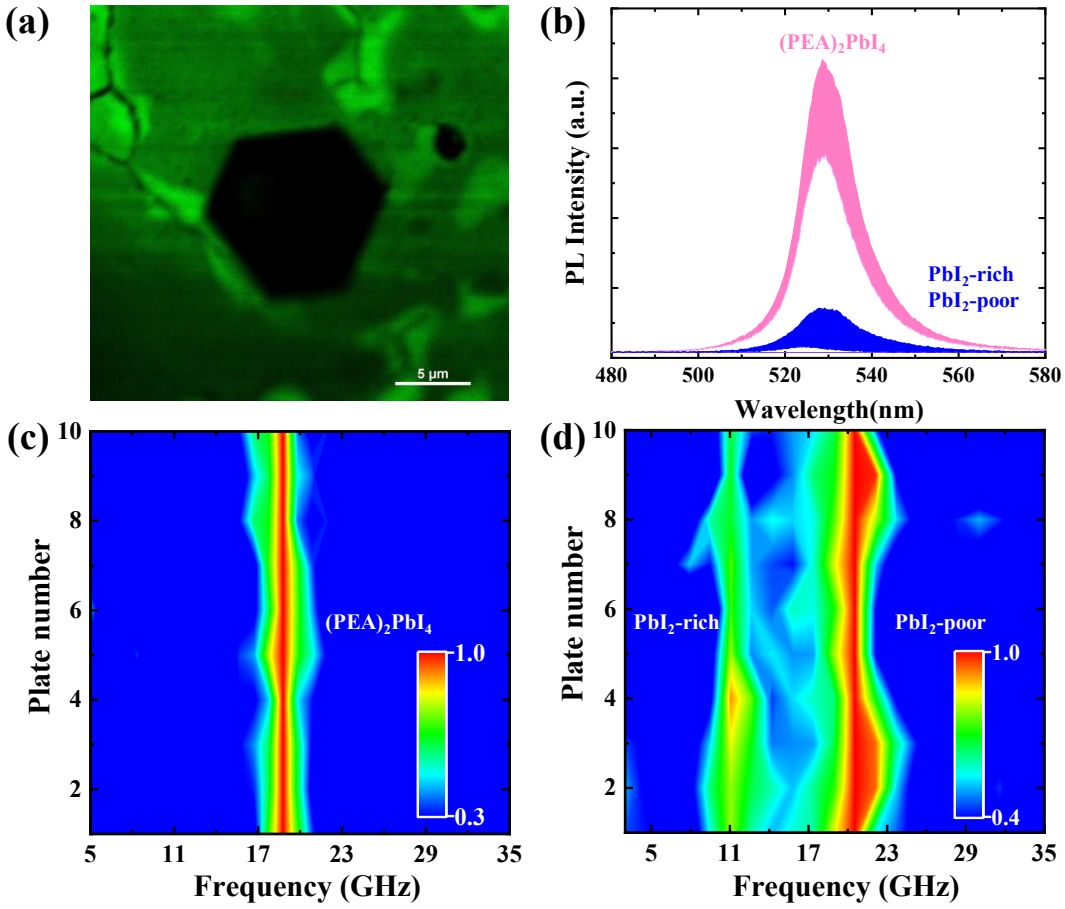

Figure 3: Correlation between Brillouin oscillations and PL intensities for the characterization of structural heterogeneity.
(a) PL imaging of an area with a single Au NPL on top of $(PEA)_2PbI_4$ film. (b) Variations of PL intensity of $(PEA)_2PbI_4$ film at different locations where bright (PL intensity in top 20%) and dim (PL intensity in bottom 20%) areas were selected for Brillouin spectroscopy measurements. (c) and (d) are the corresponding FFT spectra of Brillouin oscillations in areas with bright and dim PL, respectively. The frequency at ~19 GHz in (c) corresponds to pure $(PEA)_2PbI_4$ where PbI_4 octahedron is preserved. The frequencies at ~11 and ~21 GHz in (d) are assigned to PbI_2-rich and PbI_2-poor phases, respectively.

to be strongly correlated to structural heterogeneities. Duim et al. have shown that ion segregations in $(PEA)_2PbI_4$ produce PbI_2-rich and PbI_2-poor phases with varied fluorescence intensities compared to pure $(PEA)_2PbI_4$ structure [47]. In the current studies, $(PEA)_2PbI_4$ perovskites with nonuniform fluorescences were also prepared and a representative fluorescence imaging is shown in Figure 3a with a mapping area of ~25 × 25 μm^2 where a hexagonal Au NPL was on top. The fluorescence spectroscopy is presented in Figure 3b for the bright (PL intensity in top 20%) and dim (PL intensity in bottom 20%) areas. The reason for this selection is to show a clear correlation between fluorescence and Brillouin oscillation frequency. Note that structural heterogeneity affects fluorescence intensity more effectively than the emission wavelength. Figure 3c and d show the corresponding FFT spectra of Brillouin oscillations in areas with bright and dim PL intensities, respectively. A single Brillouin peak at f_b = 18.6 ± 0.5 GHz was observed for the areas with bright PL, while mode splitting appeared for the areas with dim PL. The Brillouin peak at ~18.6 GHz in Figure 3c can be assigned to acoustic phonons in pure $(PEA)_2PbI_4$ phase, that is consistent with results in Figure 2. Since ion segregation in $(PEA)_2PbI_4$ films was confirmed previously by PL measurements, PbI_2-rich and PbI_2-poor phases were suggested for the structural heterogeneity [9, 47]. The split of Brillouin peak in Figure 3d could also be the formation of PbI_2-rich and PbI_2-poor phases. The calculated Brillouin frequency for pure PbI_2 phase is ~11.5 GHz by using sound velocity of ~1540 m/s and refractive index of ~2 [48, 49]. The lower frequency band at ~11 GHz in Figure 3d is close to the frequency of acoustic phonon in pure PbI_2, it is thus reasonable to label it as acoustic wave in PbI_2-rich phase. Similarly, the other higher frequency band at ~21 GHz is acoustic phonon in

PbI_2-poor phase. Not surprisingly, both the frequency bands of PbI_2-rich and PbI_2-poor phases are extremely broad due to wide stoichiometry. Determination of stoichiometry in PbI_2-rich and PbI_2-poor phases using Brillouin frequency needs further investigations. Lastly, we emphasize that the current studies of structural inhomogeneity of perovskites were limited by the imaging speed in pump–probe microscopy. Two-dimensional mapping of structural inhomogeneity using coherent acoustic phonons will provide full correlations with PL spectroscopy [17, 50].

To further confirm the PbI_2-rich and PbI_2-poor phases, we studied the dynamic phase response under light stimulus. Earlier works have shown that light can break down perovskite lattices, even in layered perovskites [9, 41, 51, 52]. Understanding the dynamic response of layered perovskites under external stresses is particularly interesting from both application and fundamental standpoints. Figure 4a shows the Brillouin oscillations of $(PEA)_2PbI_4$ film after continuously exposing to pulsed laser light for several minutes. A shifting of the Brillouin oscillations was clearly observable and the corresponding FFT spectra are shown in Figure 4b. The results show that the PbI_2-poor phase with Brillouin frequency at ~25 GHz was slowly disappearing with increasing light fluences, while the PbI_2-rich phase at ~11 GHz was stable and the frequency band became narrower indicating the gradual formation of PbI_2 phase. Previously, Fang et al. have shown that light can induce degradation of $(PEA)_2PbI_4$ perovskites via releasing of PEA + HI, and leaving PbI_2 phase in the crystals [9]. Observations of the disappearance of PbI_2-poor phase and the formation of PbI_2 phase using coherent acoustic phonons also confirm the light-induced degradations in 2D perovskites. Compared to the PL intensity measurements, assignment of structural changes based on the frequency shift of Brillouin oscillations presents a direct measurement.

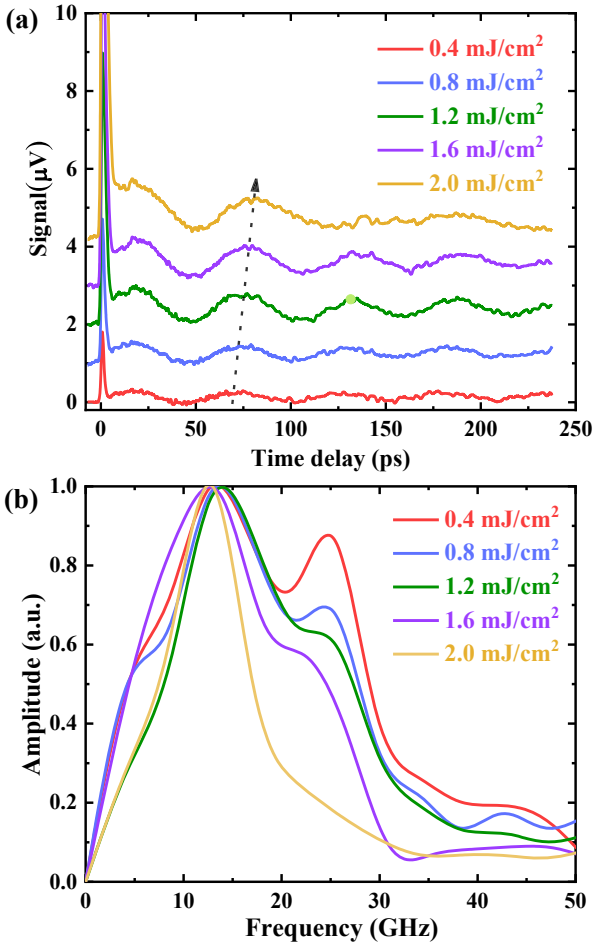

Figure 4: Light induced ion migration monitored with coherent acoustic phonons.
(a) Transient reflectivity traces show the Brillouin oscillations at varied pump fluences from 0.4–2 mJ/cm^2. The traces were shifted vertically for a clear vision. (b) The corresponding FFT spectra show the gradual formation of PbI_2 phase at frequency of ~11 GHz and slowly disappearing of PbI_2-poor phase at frequency of ~25 GHz.

Coherent acoustic phonons are less explored in perovskites, especially in 2D RP layered perovskites. High quality single crystal perovskites were mainly used due to the improved stability. However, understanding acoustic phonon properties for thin film perovskites will be particularly interesting for its practical applications, such as solar cells [4, 6, 26]. It is also a prerequisite to excite the crystals with energies above-bandgap to generate coherent acoustic phonons in perovskites. Using plasmonic metal nanostructures as optoacoustic transducers to generate coherent acoustic waves in perovskites will mitigate these limitations. Exploring time-domain Brillouin spectroscopy for the study of coherent acoustic phonons in thin film perovskites presents an exciting aspect.

Guo et al. and Maity et al. have investigated the generation and propagation of coherent acoustic phonons along the cross-plane direction of 2D RP perovskites using pump-probe spectroscopy [36, 43]. The probe wavelengths were tuned away from optical bandgap to reduce attenuations in order to have a deep penetration depth and a long phonon lifetime. It can also be interesting to study the coherent acoustic phonons with probe at optical bandgap where structural heterogeneity is detectable. Compared to many other spectroscopy techniques, time-resolved Brillouin microscopy provides an additional toolbox to study structural and elastic heterogeneity in perovskites. Furthermore, coherent acoustic phonons can be applied to dynamically monitor structural evolution under external stresses. However, the sensitivity of coherent acoustic phonons to structural heterogeneity needs further improvement due to the broad acoustic phonons bandwidth.

3 Conclusions

In the current studies, metallic Au NPLs were used as opto-acoustic transducers to facilitate the generation of coherent acoustic phonons in 2D RP $(PEA)_2PbI_4$ perovskites. A longitudinal sound velocity $v = 1937 \pm 31$ m/s along the cross-plane direction was measured, which is lower than that of 3D perovskites. Mechanical properties were obtained from the sound velocity. We calculated an elastic modulus $E = 9.84$ GPa along the cross-plane direction for $(PEA)_2PbI_4$ perovskites. Analyzing the phonon propagation in 2D RP perovskites with a bead-spring model, we obtained a spring constant of $k \approx 1.709$ N m^{-1} for PEA cations which is slightly larger than BA cations in $(CH_3(CH_2)_3NH_3)_2PbI_4$ perovskites. The small value is consistent with the low sound velocity and poor thermal conductivity in 2D layered perovskites. We further applied coherent acoustic phonons to differentiate structural heterogeneity in $(PEA)_2PbI_4$ perovskites and monitor dynamic phase evolution under light stimulus. PbI_2-rich phase and PbI_2-poor phase were both observed and the results were consistent with PL measurements. In particular, realizing dynamic structure examination in perovskites will help the understanding and tuning structural dependent properties.

4 Experimental methods

Materials. $HAuCl_4 \cdot 3H_2O$, 1-pentanol, poly(vinylpyrrolidone) (PVP, Mw = 40,000), cetyltrimethylammonium bromide (CTAB, ≥99%) lead (II) iodide (PbI_2, >99.99%), phenyl-ethyl ammonium iodine (PEAI, 99%), *N*, *N*-dimethylformamide (DMF) were purchased from Sigma-Aldrich (USA). Ethanol (AR, ≥99.7%), dichloromethane (AR, ≥99.5%) were purchased from Shanghai Chemical Reagent Company. Glass coverslips (catalog no. CG15KH) were purchased from Thorlabs China. All chemicals were used as received without purification.

Synthesis of Au nanoplates. The Au NPLs were synthesized using a modified method [35]. Briefly, 60 mg PVP and 25 mg CTAB were dissolved in 10 mL 1-pentanol solution. 0.167 mL $HAuCl_4$ (0.1 M) 1-pentanol solution and 0.5 mL ultrapure water were added to the solution. The above mixture was heated to 120 °C and maintained for 24 h to facilitate the growth of Au NPLs. The solution was cooled to room temperature and the samples were washed with ethanol at least three times by centrifugation to remove excessive surfactants. The final Au NPLs were kept at dichloromethane before the deposition on surface of perovskite films.

Synthesis of 2D perovskite films. The synthesis procedure was modified from previous report [14]. Phenethylammonium iodide (498 mg) and PbI_2 (461 mg) were dissolved in DMF (1.5 mL) at 70 °C and the solution was kept stirring for 1 h. Glass substrates for supporting the perovskite films were cleaned with acetone, ethanol, and water in the ultrasonic bath for 20 min in each solvent and then cleaned with oxygen plasma for another 20 min. 10 μL of the prepared solution was spin-coated on the glass substrate. The perovskite film was obtained by heating the substrate at 70 °C for 20 min. The Au NPLs in dichloromethane were deposited on the perovskite films by drop-casting. Note that dichloromethane does not affect the integrity of the perovskite films. The perovskite films were characterized by absorption, photoluminescence and X-ray diffraction spectroscopy. The propagation of coherent acoustic phonons in perovskites was studied by transient absorption microscopy.

Transient absorption microscopy. The coherent acoustic phonons in perovskite films were launched by exciting single Au NPLs with a pump beam and detected by a probe beam in a pump–probe scheme. Specifically, the measurements were performed with a Coherent Mira 900 Ti:sapphire laser system, which gives an output power of ~4.5 W at 800 nm with ~76 MHz repetition rate and ~100 fs pulse width. The output laser beam was split with a 80/20 beamsplitter. The weaker portion was modulated by an acousto-optical modulator (IntraAction AOM-402AF3) at 1 MHz before exciting the samples, that was triggered by the internal function generator of a lock-in amplifier (Stanford Research Systems SR844). The stronger portion of the laser beam was designed to pump an optical parametric oscillator (Coherent Mira OPO) to give a visible probe light. The pump and probe beams were spatially overlapped with a dichroic mirror and focused at the sample with an Olympus 60 × 0.9 numerical aperture (NA) microscope objective. A Thorlabs DDS600 linear translation stage was used to control the time delay between the pump and probe beams. A Hamamatsu C12702-11 avalanche photodiode was used to detect the reflected probe light. Typical powers were 2.5 mW and 50 μW for the pump and probe, respectively. The measurements were conducted under ambient conditions.

Author contribution: All the authors have accepted responsibility for the entire content of this submitted manuscript and approved submission.

Research funding: National Natural Science Foundation of China (grant 11734012, 12074266, 12074267), Science and Technology Project of Guangdong (grant 2020B010190001) and Shenzhen (grant 20200802180159001).

Conflict of interest statement: The authors declare no competing financial interest.

References

[1] H. Wang, X. Zhang, Q. Wu, et al., "Trifluoroacetate induced small-grained $CsPbBr_3$ perovskite films result in efficient and stable light-emitting devices," *Nat. Commun.*, vol. 10, p. 665, 2019.

[2] M. A. Green, A. Ho-Baillie, and H. J. Snaith, "The emergence of perovskite solar cells," *Nat. Photonics*, vol. 8, pp. 506–514, 2014.

[3] J. Wang, J. Li, S. Lan, et al., "Controllable growth of centimeter-sized 2D perovskite heterostructures for highly narrow dual-band photodetectors," *ACS Nano*, vol. 13, pp. 5473–5484, 2019.

[4] Z. Yang, Z. Yu, H. Wei, et al., "Enhancing electron diffusion length in narrow-bandgap perovskites for efficient monolithic perovskite tandem solar cells," *Nat. Commun.*, vol. 10, p. 4498, 2019.

[5] Y. P. Fu, H. M. Zhu, C. C. Stoumpos, et al., "Broad wavelength tunable robust lasing from single-crystal nanowires of cesium lead halide perovskites (CsPbX3, X= Cl, Br, I)," *ACS Nano*, vol. 10, pp. 7963–7972, 2016.

[6] Z. Li, T. R. Klein, D. H. Kim, et al., "Scalable fabrication of perovskite solar cells," *Nat. Rev. Mater.*, vol. 3, p. 18017, 2018.
[7] R. Wang, M. Mujahid, Y. Duan, Z. Wang, J. Xue, and Y. Yang, "A review of perovskites solar cell stability," *Adv. Funct. Mater.*, vol. 29, p. 1808843, 2019.
[8] J. C. Blancon, H. Tsai, W. Nie, et al., "Extremely efficient internal exciton dissociation through edge states in layered 2D perovskites," *Science*, vol. 355, pp. 1288–1291, 2017.
[9] H. Fang, J. Yang, S. Tao, et al., "Unravelling light-induced degradation of layered perovskite crystals and design of efficient encapsulation for improved photostability," *Adv. Funct. Mater.*, vol. 28, p. 1800305, 2018.
[10] H. Ren, S. D. Yu, L. F. Chao, et al., "Efficient and stable Ruddlesden-Popper perovskite solar cell with tailored interlayer molecular interaction," *Nat. Photonics*, vol. 14, pp. 154–163, 2020.
[11] A. O. El-Ballouli, O. M. Bakr, and O. F. Mohammed, "Structurally tunable two-dimensional layered perovskites: from confinement and enhanced charge transport to prolonged hot carrier cooling dynamics," *J. Phys. Chem. Lett.*, vol. 11, pp. 5705–5718, 2020.
[12] F. Thouin, A. R. S. Kandada, D. A. Valverde-Chavez, et al., "Electron-phonon couplings inherent in polarons drive exciton dynamics in two-dimensional metal-halide perovskites," *Chem. Mater.*, vol. 31, pp. 7085–7091, 2019.
[13] J. Yin, P. Maity, R. Naphade, et al., "Tuning hot carrier cooling dynamics by dielectric confinement in two-dimensional hybrid perovskite crystals," *ACS Nano*, vol. 13, pp. 12621–12629, 2019.
[14] A. Fieramosca, L. Polimeno, V. Ardizzone, et al., "Two-dimensional hybrid perovskites sustaining strong polariton interactions at room temperature," *Sci. Adv.*, vol. 5, p. eaav9967, 2019.
[15] K. Miyata, D. Meggiolaro, M. T. Trinh, et al., "Large polarons in lead halide perovskites," *Sci. Adv.*, vol. 3, p. e1701217, 2017.
[16] I. Mela, C. Poudel, M. Anaya, et al., "Revealing nanomechanical domains and their transient behavior in mixed-halide perovskite films," *Adv. Funct. Mater.*, vol. 31, p. 2100293, 2021.
[17] E. M. Tennyson, T. A. S. Doherty, and S. D. Stranks, "Heterogeneity at multiple length scales in halide perovskite semiconductors," *Nat. Rev. Mater.*, vol. 4, pp. 573–587, 2019.
[18] D. W. deQuilettes, S. M. Vorpahl, S. D. Stranks, et al., "Impact of microstructure on local carrier lifetime in perovskite solar cells," *Science*, vol. 348, pp. 683–686, 2015.
[19] M. J. Simpson, B. Doughty, S. Das, K. Xiao, and Y. Z. Ma, "Separating bulk and surface contributions to electronic excited-state processes in hybrid mixed perovskite thin films via multimodal all-optical imaging," *J. Phys. Chem. Lett.*, vol. 8, pp. 3299–3305, 2017.
[20] M. E. Stuckelberger, T. Nietzold, B. M. West, et al., "Effects of X-rays on perovskite solar cells," *J. Phys. Chem. C*, vol. 124, pp. 17949–17956, 2020.
[21] M. Kodur, R. E. Kumar, Y. Q. Luo, et al., "X-Ray microscopy of halide perovskites: techniques, applications, and prospects," *Adv. Energy Mater.*, vol. 10, p. 1903170, 2020.
[22] I. V. Kabakova, I. Azuri, Z. Y. Chen, et al., "The effect of ionic composition on acoustic phonon speeds in hybrid perovskites from Brillouin spectroscopy and density functional theory," *J. Mater. Chem. C*, vol. 6, pp. 3861–3868, 2018.
[23] R. Chatterjee, I. M. Pavlovetc, K. Aleshire, G. V. Hartland, and M. Kuno, "Subdiffraction infrared imaging of mixed cation perovskites: probing local cation heterogeneities," *ACS Energy Lett.*, vol. 3, pp. 469–475, 2018.
[24] V. E. Gusev and P. Ruello, "Advances in applications of time-domain Brillouin scattering for nanoscale imaging," *Appl. Phys. Rev.*, vol. 5, p. 031101, 2018.
[25] R. Prevedel, A. Diz-Munoz, G. Ruocco, and G. Antonacci, "Brillouin microscopy: an emerging tool for mechanobiology," *Nat. Methods*, vol. 16, pp. 969–977, 2019.
[26] J. F. Yang, X. M. Wen, H. Z. Xia, et al., "Acoustic-optical phonon up-conversion and hot-phonon bottleneck in lead-halide perovskites," *Nat. Commun.*, vol. 8, p. 14120, 2017.
[27] T. Debnath, D. Sarker, H. Huang, et al., "Coherent vibrational dynamics reveals lattice anharmonicity in organic-inorganic halide perovskite nanocrystals," *Nat. Commun.*, vol. 12, p. 2629, 2021.
[28] M. Fu, P. Tamarat, J. B. Trebbia, et al., "Unraveling exciton-phonon coupling in individual $FAPbI_3$ nanocrystals emitting near-infrared single photons," *Nat. Commun.*, vol. 9, p. 3318, 2018.
[29] K. Yu, T. Devkota, G. Beane, G. P. Wang, and G. V. Hartland, "Brillouin oscillations from single Au nanoplate opto-acoustic transducers," *ACS Nano*, vol. 11, pp. 8064–8071, 2017.
[30] C. Thomsen, H. T. Grahn, H. J. Maris, and J. Tauc, "Surface generation and detection of phonons by picosecond light pulses," *Phys. Rev. B*, vol. 34, pp. 4129–4138, 1986.
[31] P. Narum, A. L. Gaeta, M. D. Skeldon, and R. W. Boyd, "Instabilities of laser beams counterpropagating through a Brillouin-active medium," *J. Opt. Soc. Am. B*, vol. 5, pp. 623–628, 1988.
[32] F. Yang, T. J. Grimsley, S. Che, G. A. Antonelli, H. J. Maris, and A. V. Nurmikko, "Picosecond ultrasonic experiments with water and its application to the measurement of nanostructures," *J. Appl. Phys.*, vol. 107, p. 103537, 2010.
[33] V. S. Chirvony, I. Suárez, J. Rodríguez-Romero, et al., "Inhomogeneous broadening of photoluminescence spectra and kinetics of nanometer-thick $(phenethylammonium)_2PbI_4$ perovskite thin films: implications for optoelectronics," *ACS Appl. Nano Mater.*, vol. 4, pp. 6170–6177, 2021.
[34] G. El-Hajje, C. Momblona, L. Gil-Escrig, et al., "Quantification of spatial inhomogeneity in perovskite solar cells by hyperspectral luminescence imaging," *Energy Environ. Sci.*, vol. 9, pp. 2286–2294, 2016.
[35] K. Yu, Y. Yang, J. Z. Wang, G. V. Hartland, and G. P. Wang, "Nanoparticle-fluid interactions at ultrahigh acoustic vibration frequencies studied by femtosecond time-resolved microscopy," *ACS Nano*, vol. 15, pp. 1833–1840, 2021.
[36] P. J. Guo, C. C. Stoumpos, L. L. Mao, et al., "Cross-plane coherent acoustic phonons in two-dimensional organic-inorganic hybrid perovskites," *Nat. Commun.*, vol. 9, p. 2019, 2018.
[37] W. Liu, J. Xing, J. Zhao, et al., "Giant two-photon absorption and its saturation in 2D organic-inorganic perovskite," *Adv. Opt. Mater.*, vol. 5, p. 1601045, 2017.
[38] M. Wang, J. Tang, H. Wang, C. Zhang, Y. S. Zhao, and J. N. Yao, "Grain boundary enhanced photoluminescence anisotropy in two-dimensional hybrid perovskite films," *Adv. Opt. Mater.*, vol. 8, p. 1901780, 2020.
[39] K. Du, Q. Tu, X. Zhang, et al., "Two-dimensional lead(II) halide-based hybrid perovskites templated by acene alkylamines: crystal structures, optical properties, and piezoelectricity," *Inorg. Chem.*, vol. 56, pp. 9291–9302, 2017.
[40] K. T. Cho, G. Grancini, Y. Lee, et al., "Selective growth of layered perovskites for stable and efficient photovoltaics," *Energy Environ. Sci.*, vol. 11, pp. 952–959, 2018.

[41] Q. Shang, Y. Wang, Y. Zhong, et al., "Unveiling structurally engineered carrier dynamics in hybrid quasi-two-dimensional perovskite thin films toward controllable emission," *J. Phys. Chem. Lett.*, vol. 8, pp. 4431–4438, 2017.
[42] J. Wang, K. Yu, Y. Yang, G. V. Hartland, J. E. Sader, and G. P. Wang, "Strong vibrational coupling in room temperature plasmonic resonators," *Nat. Commun.*, vol. 10, p. 1527, 2019.
[43] P. Maity, J. Yin, B. Cheng, J. H. He, O. M. Bakr, and O. F. Mohammed, "Layer-dependent coherent acoustic phonons in two-dimensional Ruddlesden-Popper perovskite crystals," *J. Phys. Chem. Lett.*, vol. 10, pp. 5259–5264, 2019.
[44] P. A. Mante, C. C. Stoumpos, M. G. Kanatzidis, and A. Yartsev, "Electron-acoustic phonon coupling in single crystal $CH_3NH_3PbI_3$ perovskites revealed by coherent acoustic phonons," *Nat. Commun.*, vol. 8, p. 14398, 2017.
[45] S. J. Zhang, P. Audebert, Y. Wei, et al., "Preparations and characterizations of luminescent two dimensional organic-inorganic perovskite semiconductors," *Materials*, vol. 3, pp. 3385–3406, 2010.
[46] M. H. Jung, "Exploration of two-dimensional perovskites incorporating methylammonium for high performance solar cells," *Cryst. Eng. Comm*, vol. 23, pp. 1181–1200, 2021.
[47] H. Duim, S. Adjokatse, S. Kahmann, G. H. ten Brink, and M. A. Loi, "The impact of stoichiometry on the photophysical properties of Ruddlesden-Popper perovskites," *Adv. Funct. Mater.*, vol. 30, p. 1907505, 2020.
[48] R. Ran, C. Cheng, Z. Y. Zeng, X. R. Chen, and Q. F. Chen, "Mechanical and thermal transport properties of monolayer PbI_2 via first-principles investigations," *Philos. Mag. A*, vol. 99, pp. 1277–1296, 2019.
[49] A. Ahmad, S. Saq'an, B. Lahlouh, M. Hassan, A. Alsaad, and H. El-Nasser, "Ellipsometric characterization of PbI_2 thin film on glass," *Physica B*, vol. 404, pp. 1–6, 2009.
[50] Y. Z. Wang, D. H. Hurley, Z. L. Hua, et al., "Imaging grain microstructure in a model ceramic energy material with optically generated coherent acoustic phonons," *Nat. Commun.*, vol. 11, p. 1597, 2020.
[51] M. C. Brennan, S. Draguta, P. V. Kamat, and M. Kuno, "Light-induced anion phase segregation in mixed halide perovskites," *ACS Energy Lett.*, vol. 3, pp. 204–213, 2018.
[52] C. C. Boyd, R. Cheacharoen, T. Leijtens, and M. D. McGehee, "Understanding degradation mechanisms and improving stability of perovskite photovoltaics," *Chem. Rev.*, vol. 119, pp. 3418–3451, 2019.

Supplementary Material: The online version of this article offers supplementary material (https://doi.org/10.1515/nanoph-2021-0358).